Aging and intraocular pressure homeostasis in mice

Guorong Li[1], Joseph van Batenburg-Sherwood[2], Babak N. Safa[3], Nina Sara Fraticelli Guzmán[5,6], Andrea Wilson[1], Mohammad Reza Bahrani Fard[3], Kevin Choy[4], Michael L.De Ieso[1], J. Serena Cui[1], Andrew J Feola[4,5,7], Tara Weisz[1], Megan Kuhn[1], Catherine Bowes Rickman[1], Sina Farsiu[1,4]*, C. Ross Ethier[3,5]* and W. Daniel Stamer[1,4]*

[1]Department of Ophthalmology, Duke University

[2]Department of Bioengineering, Imperial College London

[3]Wallace H. Coulter Department of Biomedical Engineering, Georgia Institute of Technology and Emory University

[4]Department of Biomedical Engineering, Duke University

[5]Department of Ophthalmology, Emory University

[6] George W. Woodruff School of Mechanical Engineering, Georgia Institute of Technology, Atlanta, GA, USA

[7]Center for Visual & Neurocognitive Rehabilitation, Atlanta VA Medical Center

*Co-corresponding authors

Key words: Aqueous humor, Outflow facility, Schlemm's canal, Trabecular meshwork

Running title: Aging and outflow function

Contact information:

W. Daniel Stamer, dan.stamer@duke.edu

C. Ross Ethier, ross.ethier@bme.gatech.edu

Abstract

Age and elevated intraocular pressure (IOP) are the two primary risk factors for glaucoma, an optic neuropathy that is the leading cause of irreversible blindness. In most people, IOP is tightly regulated over a lifetime by the conventional outflow tissues. However, the mechanistic contributions of age to conventional outflow dysregulation, elevated IOP and glaucoma are unknown. To address this gap in knowledge, we studied how age affects the morphology, biomechanical properties and function of conventional outflow tissues in C57BL/6 mice, which have an outflow system similar to humans. As reported in humans, we observed that IOP in mice was maintained within a tight range over their lifespan. Remarkably, despite a constellation of age-related changes to the conventional outflow tissues that would be expected to hinder aqueous drainage and impair homeostatic function (decreased cellularity, increased pigment accumulation, increased cellular senescence and increased stiffness), outflow facility, a measure of conventional outflow tissue fluid conductivity, was stable with age. We concluded that the murine conventional outflow system has significant functional reserve in healthy eyes. However, these age-related changes, when combined with other underlying factors, such as genetic susceptibility, are expected to increase risk for ocular hypertension and glaucoma.

Introduction

Age and elevated intraocular pressure (IOP) are the two primary risk factors for glaucoma [1-6], the leading cause of irreversible blindness [7]. For example, glaucoma prevalence increases from 0.2% to 2.7% between the ages of 50 and 59 can reach 12.8% in those over 80 [6, 8-10]. With life expectancies increasing, it is predicted that there will be 1.5 billion people worldwide over the age of 65 by 2050 [11]. Therefore, there will be a dramatic increase in the incidence of glaucoma in the years to come.

Both the incidence of glaucoma and its progression are associated with ocular hypertension [12-20]. While IOP depends on several factors, it is the resistance to aqueous humor outflow that largely sets IOP, and, in a healthy eye, maintains it in the normal range over a lifetime [21-30]. In other words, elevated aqueous outflow resistance causes ocular hypertension [31]. In both normotensive and hypertensive eyes, outflow resistance is (dys)regulated by the coordinated function of the trabecular meshwork (TM), a porous connective tissue, and Schlemm's canal (SC), an endothelial-lined circular fluid collecting duct in the anterior eye. These two structures (i.e., TM and SC) are the key elements of the so-called conventional outflow pathway, which conducts the majority of the aqueous humor out of the eye (Figure 1).

Despite most individuals having IOP in the normal range, age-related changes occur in the human conventional outflow pathway in both normal and glaucomatous eyes. For example, there is a steady loss of cells in the conventional outflow pathway with age that is accelerated in glaucoma [32, 33]. Matching a decrease in aqueous inflow (production) rate [20], both unconventional and conventional outflow drainage rates decrease with age [34, 35]. Aging is an inevitable and complex multifactorial biological process that predisposes tissues to disease [36, 37]. To better understand the complex processes that contribute to ocular hypertension and glaucoma, it is essential to know more about age-related changes in the conventional outflow tissues.

To study these complex issues, we used mice for several reasons. Mice are widely used to model human disease, including glaucoma. Importantly, conventional outflow tissues in mice are anatomically, physiologically and pharmacologically remarkably similar to humans [38-42]. Further, mice have a much shorter lifespan than humans, facilitating aging studies. Finally, the thin murine sclera allows *in vivo* imaging of outflow pathway tissues [41, 43]. Therefore, we designed a study to monitor age-related changes in the conventional outflow pathway in mice. Using mice that ranged in ages from 2 to 32 months (equivalent to 16- to 80-year-old humans), we examined conventional outflow tissue morphology, biomechanical properties and function.

Results

Eye size increased with age

We measured globe size and body mass in mice of different ages. As expected, both increased with age (Supplementary Figure 1). Interestingly, globe size increased more dramatically at early stages of life than later for both sexes. Body mass of both males and females steadily increased throughout their lifetime (Supplementary Figure 1).

Aging reduces TM cellularity, increases pigment in the TM, and increases levels of the senescence marker CDKN1A (p21) in the TM

To determine whether outflow tissue structure changes over time, anterior segments of C57 mice at different ages (from 2 to 32 months old) were processed for morphological evaluation by both light and

electron microscopy (Figure 2). Mice were grouped into 3 age cohorts: young (2-6 months old), middle-aged (8-16 months old) and elderly (25-32 months old). At the light microscopic level, the gross appearance of the conventional outflow tissues (i.e., TM beam architecture and shape of SC lumen) did not differ appreciably between the three age groups. However, we did observe greater amounts of pigment and greater numbers of pigment-laden cells in the TM of middle-aged and elderly mice vs. young mice. To quantify these morphological changes, we examined transmission electron micrographs. Treating age as a continuous variable, we quantified the number of cells in the TM and observed a steady and significant decline in cell density of -2.0 [-2.8,-1.3] cells/mm^2/month (R^2 = 0.66, $p < 10^{-3}$; Figure 2G). In the same samples, we also counted the number pigment granules in the juxtacanalicular tissue (JCT; here defined as being within 7 µm of the inner wall of SC), observing an age-dependent increase in pigment granule density of 6.8 [1.7,11.9] pigment granules/mm^2/month (R^2 = 0.32, $p < 0.05$; Figure 2H). Further, the cells remaining within the TM displayed an age-related increase in the senescence marker, CDKN1A (p21, Figure 3).

TM tissue stiffens with age

We next tested whether these age-associated changes in the TM were accompanied by changes in TM biomechanical properties, since changes in such properties are known to occur in ocular hypertension and be associated with TM dysfunction [38, 39, 44-47]. Using high-resolution spectral-domain optical coherence tomography (OCT), we monitored deformations in conventional outflow tissues in response to increasing IOP. Since IOP-mediated changes in SC lumen dimensions depend upon TM stiffness [38, 39], we specifically monitored SC lumen dimensions over five sequential IOP steps (see sample images at 3 of these steps in Figure 4), using our custom semi-automatic segmentation algorithm to identify SC lumen from OCT images.

The relative change in SC cross-sectional area in response to IOP elevation was calculated for each animal in each of the three age groups (Figure 5A-C). For each eye the slope of the relationship between relative SC area and IOP was then calculated, with larger negative values representing greater collapse of the SC lumen due to increased IOP. After compiling the slopes for all eyes, we observed an age-dependent increase in the resistance to collapse of SC as IOP increased (R^2 = 0.55, $p < 10^{-3}$, Figure 5D). This observation suggests that TM tissues become structurally stiffer with age.

We next used forward finite element modeling to estimate TM stiffness based on fitting the computed collapse of SC lumen to observed values of relative SC collapse at pressures of 15 and 20 mmHg for each age group (Supplementary Figure 4). We computed a significant increase in the Young's Modulus of the TM with age; for example, over the IOP range from 10-15 mmHg, we estimated an age-associated increase of Young's modulus of 28-37% in middle-aged vs. young mice, and of 273-285% in elderly vs. young mice). Interestingly, this stiffening behavior appeared nonlinear, i.e. there was accelerated stiffening with age (Supplemental Table 1, Supplemental Figure 2, Figure 5E).

Outflow facility and IOP are stable with age

Despite the loss of cells, increased deposition of pigment and increased TM tissue stiffness, IOP was remarkably insensitive to age in mice (R^2 = 0.00, $p > 0.05$, Figure 6A). To specifically evaluate how physical changes in the TM with age affected its function, we used a specially designed system (iPerfusion) to measure the hydraulic conductance of the TM tissues (outflow facility) in enucleated eyes from mice of different ages [48]. Although we observed a gradual increase in outflow facility with age, the correlation was weak and when corrected for multiple comparisons the slope was not statistically different from zero, albeit this was borderline ($R^2 = 0.20$, $p_B > 0.05$, Figure 6B). When adjusting for the increase in the filtering area of the outflow pathway with age (due to increased globe size), the

correlation between age and adjusted outflow facility remained weak but was borderline statistically different from zero (R^2 = 0.26, $p_B < 0.05$, Supplemental Figure 3A).

Age alters the response of anterior chamber structures to IOP

Using OCT imaging, we also monitored iris deformations in response to stepwise increases of IOP (Figure 7). We observed that although the irides of older eyes were more posteriorly located at a low IOP of 10 mmHg vs. in young and middle-aged eyes (Figure 7A), the irides in young eyes were more susceptible to posterior deformation and bowing as IOP increased vs. in older eyes. To quantify this effect, we measured the angle between the iris and cornea for each animal from OCT scans, and for all cases observed an increase in this subtended angle with increasing IOP that appeared reversible when returning to a 10 mmHg baseline IOP (Figure 7B-D). From these observations, we further quantified how the baseline angle (at 10 mmHg) varied with age, and found an average increase of 0.9 [0.5,1.4] °/month (R^2 = 0.55, $p < 10^{-3}$, Figure 7E). Further, we observed that the sensitivity to changes in IOP decreased with age and quantified this effect through a constant of proportionality, ζ, between the change in angle and the change in pressure from baseline. We observed a weak correlation between ζ and age (R^2 = 0.33, p < 0.05, Figure 7F), which is consistent with structural stiffening of the iris.

The mechanical responses of anterior segment tissues in *ex vivo* eyes to increasing IOP was also analyzed by calculating the non-linearity in the pressure-flow curves obtained during perfusions of enucleated eyes, characterized by the parameter β [48]. Specifically, larger β values are thought to be associated with more posterior iris/lens movement during cannulation of the anterior chamber (i.e., anterior chamber deepening) [49]. Interestingly, we observed that β decreased in an age-dependent manner, with an average reduction of -0.027 ± [-0.039, -0.015] per month, and the correlation between β and age was R^2 = 0.51 ($p_B < 0.001$, Figure 8A). These data indicate that β is effectively zero in elderly eyes. Similarly, a strong inverse correlation was observed between adjusted ocular compliance and age (R^2 = 0.82, $p_B < 0.001$, Figure 8B), a measure of ocular coat distensibility, indicating that the corneoscleral shell stiffens with age. Even without adjustment for changes in ocular diameter with age, the correlation between ocular compliance and age was still observed (R^2 = 0.56, $p_B < 0.001$, Supplemental Figure 3B).

Discussion

In the present study, we examined a number of age-related changes in the conventional outflow tissues of mice, responsible for regulating IOP. With age, we observed an increase in pigment and pigment-laden cells in the conventional outflow pathway, but a decrease in the total number of cells and increased levels of the senescence marker CDKN1A (p21). These morphological changes were accompanied by alterations in the biomechanical properties of associated ocular tissues, which included stiffening of the TM, decreased pressure-induced deepening of the anterior chamber and decreased ocular compliance. Despite this myriad of age-related changes in the eye, especially in the outflow tissues, outflow facility remained stable or even increased slightly with age to maintain a constant IOP over the life of the mice. Thus, much like humans, the healthy mouse eye appears to adapt to age-related changes to maintain IOP within a narrow range over a lifetime [50, 51], reinforcing the idea that homeostatic feedback loop(s) regulate IOP [52, 53].

We observed more pigment and fewer cells in TM tissues, especially in the JCT area, with increasing age. These results are strikingly similar to age-related changes in the human TM, which also shows more pigment and fewer cells with age [32, 33, 54, 55] Significantly, there are even fewer TM cells and more pigment in glaucomatous eyes compared to age-matched controls [32, 54]. These results suggest a reduced capacity of TM cells, and possibly resident macrophages, to process pigment that is released by

166 the iris and other ocular pigmented epithelia. The TM functions as a biological filter, and thus a primary
167 role for the TM cells is to neutralize oxidants and phagocytose cellular debris carried by the flow of
168 aqueous humor into the TM [56-58]. TM cells are assisted in this function by resident macrophages.
169 Consistent with this understanding, we observed more pigment-laden cells in older (>12-month-old)
170 mouse eyes. The remaining TM cells in older eyes showed signs of senescence (i.e., increased CDKN1A
171 expression), possibly due to increased phagocytic and oxidative loads [59]. CDKN1A is a cyclin-
172 dependent kinase inhibitor that is a major target of p53 activity and thus is associated with linking DNA
173 damage to cell cycle arrest [60].

174 Accompanying these morphological alterations in the TM with age, the biomechanical properties of
175 ocular tissues, including the TM, also changed. Using our novel combination of OCT imaging of outflow
176 tissues subjected to varying IOP and finite element modeling, we observed significant stiffening of the
177 TM with age. Values for Young's modulus obtained for the TM were consistent with our previous
178 reports [38, 61]. For example, over the IOP range 10-15 mmHg, we estimated TM stiffnesses of 22.1-
179 26.9 kPa in young mice in the present study, which was similar to the 22-29 kPa estimated previously in
180 a young cohort. While age-induced stiffening of the TM has not been examined previously in human
181 eyes, the TM has been shown to be stiffer in glaucomatous eyes compared to age-matched controls [44,
182 45, 62, 63]. Such changes in biomechanical properties can be induced in non-glaucomatous human TM
183 cells or in the TM of young mice by prolonged glucocorticoid treatment [39]. Using our new finite
184 element model that accounts for physical changes in the eye with age, we estimated a TM stiffness of
185 85.2-100.5 kPa over the IOP range 10-15 mmHg for our elderly cohort in the present study, which is
186 greater than the estimated stiffness of 69 kPa for a younger cohort of mice with steroid-induced ocular
187 hypertension [38].

188 Taken together, these data suggest important differences between normal age-associated changes and
189 pathological changes to the TM. More specifically, increased TM tissue stiffness positively correlates
190 with a *decrease* in outflow facility in young mice under pathological conditions [45], while in the present
191 study, we saw that both TM stiffness and outflow facility *increased* (albeit slightly) with age. This
192 apparent paradox may be due to differences in disease versus normal aging, both of which result in TM
193 stiffening but by different biological mechanisms. For example, there was an increase in basal laminar
194 deposits below the inner wall of SC in young mice experiencing glucocorticoid-induced ocular
195 hypertension and TM stiffening [39], whereas in the present study we observed the normal "patchy"
196 basal laminar materials below the inner wall of SC in elderly mice with a stiffer TM.

197 Part of the increase in facility can be attributed to age-related morphological changes such as increased
198 globe size, and thus a corresponding increase in TM cross-sectional area with age (Figure 6B and
199 Supplementary Figure 3A) [64]. However, even after adjusting for TM area, there was still a slight, but
200 significant increase in facility, which we speculate may be a compensatory effect associated with
201 decreased unconventional outflow with age, as seen in non-human primates. This would result in a
202 shunting of flow from the unconventional to the conventional outflow tract [65], which in turn would
203 require an increase in facility to maintain a desired IOP. Such an increase is consistent with two previous
204 studies that examined outflow facility in aging mice; each reported an increase, or a trend towards an
205 increase, in outflow facility in 3 of 4 strains studied, including C57 mice [66, 67].

206 In addition to increased TM tissue stiffness, we observed other age-related changes in ocular tissue
207 biomechanical properties. For example, we monitored posterior iridial bowing due to increasing IOP.
208 Like TM tissues, the pressure-induced posterior displacement of the iris was decreased with age,
209 indicating increased iridial structural stiffness. These results are consistent with a decreased β that was
210 observed in older eyes during ocular perfusions in the present study. Beta is the constant of
211 proportionality between relative changes in facility and relative changes in pressure [49], and a smaller

212 β is consistent with less posterior displacement of the iris and lens as IOP increases, likely due to
213 increased ocular tissue stiffness. Lastly, we observed decreased ocular compliance with age. Even when
214 adjusted for increased globe size with age, compliance was still significantly smaller in older eyes. These
215 three indicators of changes in ocular tissue properties with age are consistent with an abundant
216 literature demonstrating that age decreases tissue elasticity and increases tissue stiffness in many other
217 tissues such as skin, lungs, and blood vessels [37].

218 In summary, we provide the first comprehensive study reporting the effects of age on the properties
219 and function of conventional outflow tissues. As the primary determinant of intraocular pressure (and
220 thus playing a critical role in ocular hypertension and glaucoma), it is important to understand how the
221 function and morphology of outflow tissues change with age. The changes we describe here provide a
222 physiological backdrop for susceptibility to genetic or environmental insults that result in outflow
223 dysfunction/loss of IOP homeostasis, elevated IOP and glaucoma.

224 Methods

225 **Animals**

226 A total of 213 C57BL/6 (C57) mice (both males and females, ages 2-32 months) were used in this study
227 for the various measurements performed. It was not possible to conduct all reported measurements on
228 each mouse (histology, OCT imaging, perfusion), and thus each type of experiment was conducted on a
229 subset of the 213 mice, so that age ranges reported in graphs and tables may not span the entire range
230 from 2-32 months. All mice were handled in accordance with approved protocols (A001-19-01 and
231 A226-21-11; Duke University Institutional Animal Care and Use Committee) and in compliance with the
232 Association for Research in Vision and Ophthalmology (ARVO) Statement for the Use of Animals in
233 Ophthalmic and Vision Research. The mice were purchased from the Jackson Laboratory (Bar Harbor,
234 Maine, USA), bred/housed in clear cages and kept in housing rooms at 21°C with a 12h:12h light:dark
235 cycle.

236 **Body mass measurements**

237 An empty cage was tared on a balance (Model 1015SSTP, Taylor) after which a live mouse was put into
238 the cage and the body mass was recorded.

239 **Intraocular pressure measurements**

240 The mice were anesthetized with intraperitoneal injected ketamine (60 mg/kg) and xylazine (6 mg/kg).
241 IOP was measured immediately upon cessation of movement (i.e., under light anesthesia) using rebound
242 tonometry (TonoLab, Icare, Raleigh, NC, USA) between 10am and 1pm [38, 40, 41, 68, 69]. Each
243 recorded IOP was an average of six measurements, giving a total of 36 rebounds from the same eye per
244 recorded IOP value.

245 **Perfusion measurement of aqueous humor dynamics parameters**

246 We measured key Aqueous Humor Dynamics (AHD) parameters, namely outflow facility, beta
247 (nonlinearity factor) and ocular compliance in freshly enucleated mouse eyes using the iPerfusion
248 system as described in detail previously [38, 39, 48, 70, 71]. Briefly, mice were euthanized using
249 isoflurane gas, and eyes were carefully enucleated. Each eye was mounted on a stabilization platform in
250 the center of a temperature-regulated perfusion chamber using a small amount of cyanoacrylate glue
251 (Loctite, Westlake, OH, USA). The perfusion chambers were filled with pre-warmed Dulbecco's
252 phosphate-buffered saline with added D-glucose (DBG 5.5 mM), submerging the eyes to maintain their

hydration, and temperature at 35°C. The eyes were then cannulated using glass microneedles connected to each channel of the iPerfusion system. Using micromanipulators under a stereomicroscope, a microneedle was inserted into the anterior chamber of each eye. The eyes were perfused at 9 mmHg for 30 min to allow acclimatization and stabilization, followed by perfusion at 9 sequential pressure steps of 4.5, 6, 7.5, 9, 10.5, 12, 15, 18 and 21 mmHg. To define stability at each pressure step, the flow rate (Q) was filtered with a 60-second Savitsky-Golay filter [72], and its time derivative (the slope) was determined via linear regression analysis. Stability of pressure (P) was defined as a minute-long maintenance of the slope under 3 nl/min/min. Stable Q and P data were filtered with another 60-second Savitsky-Golay filter and averaged over 4 minutes at each pressure step for further analysis [40, 48, 69].

Outflow facility and beta (β) and their 95% confidence intervals were calculated using a non-linear data-fitting to fit the established power law model to the experimental data

$$Q = C_r \left(\frac{P}{P_r}\right)^{\beta} P$$

where C_r is the 'reference facility' measured at the reference pressure, $P_r = 8\ \mathrm{mmHg}$, chosen to represent a physiological pressure drop across the conventional outflow pathway [48].

To calculate the ocular compliance, defined as the instantaneous change in the eye volume in response to a unit change in IOP, we employed the step response method [71]. In this method, the various components of the perfusion system and the eye are modeled as analogous to electrical elements, e.g., ocular compliance and outflow facility are modeled as a capacitance and a resistance, respectively, resulting in a governing equation that relates IOP, ocular compliance and outflow facility at any given moment. This equation was fitted to the experimental pressure data to obtain ocular compliance [71]. The ocular compliance is pressure dependent, which is described by Friedenwald's equation [71], which we used to interpolate measured compliance values to a consistent reference pressure of 13 mmHg for all eyes.

Ocular diameter measurements

Since our measured AHD parameters can vary with eye size, we measured the diameter of a subset of eyes to adjust for that variability (Supplementary Figure 1). In brief, enucleated eyes were cleaned by carefully dissecting away conjunctiva and extraocular muscles. Eyes were then placed on a ruler (as a reference scale) and imaged under a dissecting microscope. The images were analyzed using ImageJ [73] software in a masked fashion, with the diameter at the ocular equator measured in millimeters.

Ocular diameter was only measured for a subset of the eyes, leading to three groups:

- Group I: Eyes in which diameter was measured but AHD parameters were not,
- Group II: Eyes in which AHD parameters were measured, but ocular diameter was not, and
- Group III: Eyes in which both diameter and AHD parameters were measured

To enable the adjustment of measured AHD parameters for ocular diameter in Group II eyes, we estimated the diameter of eyes for which the data was missing using non-linear regression. We found empirically (Figure S1) that the plot of diameter vs. age (for Groups I and III) was reasonably fit by

$$d = a_1\, Age^{\,a_2} + a_3$$

where a_1 [mm], a_2 [-] and a_3[mm] were the fitting parameters. Diameters for eyes for which d was not available were then estimated using the best fit values.

293 **Outliers and sex differences**

294 We first filtered AHD data for outliers, performed on a per-age-group basis for the logarithms of both
295 facility and compliance, since both quantities are known to be log-normally distributed [48, 71]. We
296 eliminated any data points that were more than 2.5 median absolute deviations away from the median,
297 accounting for the 95% confidence interval on the parameters [48]. This led to a single eye in the oldest
298 group being rejected based on high compliance. Data were not adjusted or stratified for sex because we
299 did not observe a statistical difference in eye size between males and females of the same age
300 (Supplemental Figure 1).

301 **Adjustment of ocular compliance and outflow facility to account for eye size**

302 Facility is expected to be dependent on the cross-sectional area of the inner wall of SC through which
303 the fluid filters. This area is equal to the circumference of the toroidal SC (approximately equal to limbal
304 circumference) multiplied by SC anterior-posterior length, both of which have been observed to increase
305 with age, but only modestly (Supplemental Figure 1 and [64]). Normalization by area would give a
306 conductivity (facility/area) with hard-to-interpret units [nl/min/mmHg/mm^2] and involve an estimate of
307 SC anterior-posterior length, which showed significant inter-animal variability [64]. Instead, we used our
308 correlation between age and ocular diameter to adjust the measured reference facility to the value that
309 would be expected for an eye of the average diameter of the eyes used in this study ($\bar{d} = 3.4\ \mathrm{mm}$). This
310 "adjusted reference outflow facility", $C_{r,i}^{a}$, for a given eye, i, is given by

311 $$C_{r,i}^{a} = C_{r,i}\left(\frac{\bar{d}}{d_i}\right)$$

312 The value $C_{r,i}^{a}$ is the adjusted facility of the eye if it were to have diameter $\bar{d}$ rather than its actual
313 diameter d_i. We plot the unadjusted facility, $C_{r,i}$, in Figure 6B, which is the physiologically relevant
314 quantity strongly influencing IOP, while the adjusted value, $C_{r,i}^{a}$, is plotted in Supplemental Figure 3A.

315 Ocular compliance is, by definition, dependent on eye volume ($\pi d^3/6$). Similar to facility, we used
316 ocular diameter to adjust the measured compliance to the compliance that the eye would have had if it
317 had diameter $\bar{d}$

318 $$\phi_{r,i}^{a} = \phi_{r,i}\left(\frac{\bar{d}}{d_i}\right)^3$$

319 where $\phi_{r,i}^{a}$ is the adjusted compliance of eye i, and $\phi_{r,i}$ is the compliance of eye i before adjustment.
320 Figure 8B plots $\phi_{r,i}^{a}$, which is a relevant measure of ocular coat (corneo-scleral shell) material properties,
321 while Supplemental Figure 3B plots the unadjusted compliance values $\phi_{r,i}$.

322 Note that since compliance and facility are both log-normally distributed, we carried out all analyses in
323 the logarithmic domain [48, 71].

324 **Optical coherence tomographic imaging**

325 *In vivo* imaging was carried out using an Envisu R2200 high-resolution spectral domain (SD)-OCT system
326 (Bioptigen Inc., Research Triangle Park, NC, USA). We followed our previously established techniques to
327 image iridocorneal angle structures in mice [38-41, 68, 70, 74]. Briefly, mice were anesthetized with
328 ketamine (100 mg/kg)/xylazine (10 mg/kg) by IP administration. While mice were secured on a custom-
329 made platform, a single pulled glass microneedle filled with phosphate buffered saline (PBS) was
330 inserted into the anterior chamber of one eye. The microneedle was connected to both a manometric
331 column to adjust IOP and a pressure transducer to continuously monitor IOP levels using PowerLab

software. The OCT imaging probe was aimed at either the nasal or temporal limbus and the image was centered and focused on the SC lumen. While collecting images, mouse eyes were subjected to a series of IOP steps (10, 12, 15, 17 and 20 mmHg) by adjusting the height of the fluid reservoir. At each IOP step, a sequence of repeated OCT B-scans (each with 1000 A-scans spanning 0.5 mm in lateral length) from spatially close positions were captured, registered and averaged to create a high signal-to-noise-ratio image of the iridocorneal angle region in each animal. The duration of each pressure step was ~1-2 minutes.

Segmentation of OCT images

OCT B-scans of iridocorneal angle tissues were registered and segmented following established methods [38-40] using SchlemmSeg software, which includes two modules: Schlemm I and Schlemm II. Briefly, OCT B-scans were automatically registered using our custom Schlemm I software for SC segmentation. The Schlemm II software package was then used to differentiate SC from scleral vessels, which were automatically marked. If SC was seen to be connected to collector channels (CC), manual separation of SC from CC was required, and was based on the shape of SC and speckling in the images generated by blood cells or other reflectors contained in blood vessels [39-41, 70, 75-78]. The speckle variance OCT-angiography images were generated based on the speckling in SC and vessels as described in detail previously [40]. SC was easily differentiated from other vessels due to its size and location.

Measurement of iris-cornea subtended angle

It was evident from OCT scans that the iris bowed and displaced posteriorly as IOP increased. To quantify this effect, we measured the angle subtended by the iris and cornea. In anesthetized mice (see above), OCT images of the anterior segment (400 x 300 pixels, corresponding to a 2 x 1.26 mm field of view [horizontal × vertical]) were imported into ImageJ, and 2-line segments, each 19 pixels long, were drawn from the apex of the irideo-corneal angle to the anterior surface of the iris and to the posterior surface of the cornea. The angle subtended between these segments was measured in ImageJ, accounting for the horizontal-to-vertical aspect ratio of the image.

Quantitative estimation of TM biomechanical properties (tissue stiffness)

The stiffness of the TM increases in glaucomatous eyes and is known to be associated with the function of the conventional outflow pathway tissues, i.e., stiffer tissues have higher flow resistance [45]. It was therefore of great interest to assess how TM stiffness changes with age. For this purpose, we used finite element modeling driven by OCT images acquired as described above. In brief, increasing IOP deforms the TM and partially collapses SC lumen; we tracked luminal collapse as the main OCT imaging outcome measure, which we then fit with our finite element model. The full modeling methodology is beyond the scope of this paper and is described elsewhere [64]. In brief, we used the FEBio finite element software [80] to simulate age-specific models, evaluating TM/SC deformations vs. IOP and adjusted TM stiffness so that finite element predictions of SC lumen partial collapse matched those observed experimentally by OCT. This approach included the effects of posterior deformations of the iris, pectinate ligaments connecting the iris and TM, and changes in posterior chamber pressure and SC luminal pressure with IOP. At IOPs of 15 and 20 mmHg, we computed a difference in normalized SC area, $\Delta nSCLA$**,** as follows.

$$\Delta nSCLA = \frac{SCLA_{\text{exp.}} - SCLA_{\text{comp.}}}{SCLA_{\,10\text{ mmHg}}}$$

where $SCLA$ is the cross-sectional area of Schlemm's canal lumen, the subscript "comp." refers to a computed result (finite element simulation), the subscript "exp." refers to an experimental result (OCT imaging), and the subscript "10 mmHg" refers to the reference value of $SCLA$ at an IOP of 10 mmHg.

$\Delta nSCLA$ is essentially a measure of how closely the computed collapse of SC lumen agrees with the experimentally observed collapse as IOP is increased. Perfect agreement corresponds to $\Delta nSCLA = 0$.

Histology and transmission electron microscopy

Mouse eyes were carefully enucleated immediately after sacrifice as described above, and immersion-fixed in 4% paraformaldehyde at 4 °C overnight. The eyes were then bisected, and the posterior segments and lenses were removed. The anterior segments were cut into four quadrants.

For immunohistochemistry studies, one quadrant was embedded into OCT and 10 µm sections were cryosectioned and immunostained with antibody against p21 (1:500 dilution, rabbit polyclonal, ab188224; Abcam). The secondary antibody was Alexa Fluor® 594 AffiniPure Goat Anti-Rabbit IgG (H+L) (Jackson ImmunoResearch Laboratories INC) at 1:500 dilution. Nuclei were stained with DAPI (1:1000), and images were captured using a Nikon Eclipse 90i confocal laser-scanning microscope (Melville). Images were collected at identical intensity and gain settings for all sections.

For histology studies, two opposite quadrants per eye were embedded in Epon, and 0.5 µm semithin sections were cut, stained with 1% methylene blue, and examined by light microscopy (Axioplan2, Carl Zeiss MicroImaging, Thornwood, NY).

For electron microscopy studies, mouse anterior quadrants were embedded in Epon resin and 65 nm sagittal ultrathin sections were cut through iridocorneal angle tissues using an ultramicrotome (LEICA EM UC6, Leica Mikrosysteme GmbH, A-1170, Wien, Austria). Sections were stained with uranyl acetate/lead citrate and examined with a JEM-1400 electron microscope (JEOL USA, Peabody, MA). In each section, cell numbers (nuclei) and cells containing engulfed pigment were counted in the entire visible TM tissue area (by JSC or GL) and pigment granules were counted within 7 µm of the inner wall of SC (by AW) in a masked fashion. The counts were normalized by the visible TM area and are presented as number of cells per mm^2 of entire TM or number of pigment particles per mm^2 of TM within 7 µm of the inner wall of SC.

Statistical analysis

We evaluated whether the AHD parameters (IOP, facility, beta and compliance) measured in paired eyes were correlated (Supplemental Figure 1). Although facility was not correlated ($p > 0.05$), pairwise correlation coefficients for IOP, beta and compliance were greater than 0.5 with $p < 0.001$; thus, measurements from individual eyes of a pair could not be treated as independent. Therefore, the bilateral averages from each pair of eyes were used to represent each animal and the confidence intervals for facility, beta and compliance were added in quadrature. There were some mice in which only one eye perfusion was successful; values measured in these eyes were included without modification (open circles in Figures 3B, 7A and 7B).

To investigate the relative change in SC area with pressure (Fig 5), linear regression with a fixed intercept at 100% was used to calculate the change in % SC area/mmHg and the corresponding 95% confidence interval for each eye (Figure 5D).

We also observed that the iris was displaced posteriorly as IOP increased, and the extent of this displacement was age-dependent. To characterize this phenomenon, we used OCT images to measure the angle subtended by the cornea and the root of the iris as a function of intraocular pressure. The increase in angle from baseline ($\theta - \theta_0$) was compared to the logarithm of the increase in pressure from baseline ($P - P_0$) using an empirical fit of the form

$$\theta - \theta_0 = \zeta \ln (P - P_0)$$

where ζ quantifies the sensitivity of irideo-corneal angle changes to pressure and the subscript "0" refers to the baseline condition of IOP = 10 mmHg.

Although three broad age groups were considered, age was treated as continuous variable. Regression was used to calculate coefficients of determination (R^2) calculated for cellularity, pigment granule density, IOP, log-transformed adjusted reference outflow facility, change in SC area per mmHg, baseline irideo-corneal angle, sensitivity of irideo-corneal angle to pressure (ζ), β and log-transformed adjusted reference ocular compliance. Regression parameters are reported as mean [95% confidence interval].

When testing compliance, outflow facility, and β, we used Bonferroni correction to adjust p-values in order to avoid increasing the risk of a type I error since three comparisons were made. Thus, for these parameters, we report $p_B = 3p$. All p-values were considered relative to α = 0.05, 0.01 or 0.001.

References

1. Di Pierdomenico, J., et al., *Age and intraocular pressure in murine experimental glaucoma.* Prog Retin Eye Res, 2021: p. 101021.
2. Iwase, A., et al., *The prevalence of primary open-angle glaucoma in Japanese: the Tajimi Study.* Ophthalmology, 2004. **111**(9): p. 1641-8.
3. Klein, B.E., et al., *Prevalence of glaucoma. The Beaver Dam Eye Study.* Ophthalmology, 1992. **99**(10): p. 1499-504.
4. Leske, M.C., et al., *The Barbados Eye Study. Prevalence of open angle glaucoma.* Arch Ophthalmol, 1994. **112**(6): p. 821-9.
5. Varma, R., et al., *Prevalence of open-angle glaucoma and ocular hypertension in Latinos: the Los Angeles Latino Eye Study.* Ophthalmology, 2004. **111**(8): p. 1439-48.
6. Wolfs, R.C., et al., *Changing views on open-angle glaucoma: definitions and prevalences--The Rotterdam Study.* Invest Ophthalmol Vis Sci, 2000. **41**(11): p. 3309-21.
7. Blindness, G.B.D., C. Vision Impairment, and S. Vision Loss Expert Group of the Global Burden of Disease, *Causes of blindness and vision impairment in 2020 and trends over 30 years, and prevalence of avoidable blindness in relation to VISION 2020: the Right to Sight: an analysis for the Global Burden of Disease Study.* Lancet Glob Health, 2021. **9**(2): p. e144-e160.
8. Leske, M.C., *Open-angle glaucoma -- an epidemiologic overview.* Ophthalmic Epidemiol, 2007. **14**(4): p. 166-72.
9. Bonomi, L., et al., *Prevalence of glaucoma and intraocular pressure distribution in a defined population. The Egna-Neumarkt Study.* Ophthalmology, 1998. **105**(2): p. 209-15.
10. de Voogd, S., et al., *Incidence of open-angle glaucoma in a general elderly population: the Rotterdam Study.* Ophthalmology, 2005. **112**(9): p. 1487-93.
11. Powell, S., M. Irnaten, and C. O'Brien, *Glaucoma - 'A Stiff Eye in a Stiff Body'.* Curr Eye Res, 2022: p. 1-9.
12. Gordon, M.O., et al., *The Ocular Hypertension Treatment Study: baseline factors that predict the onset of primary open-angle glaucoma.* Arch Ophthalmol, 2002. **120**(6): p. 714-20; discussion 829-30.
13. Le, A., et al., *Risk factors associated with the incidence of open-angle glaucoma: the visual impairment project.* Invest Ophthalmol Vis Sci, 2003. **44**(9): p. 3783-9.
14. Leske, M.C., et al., *Incidence of open-angle glaucoma: the Barbados Eye Studies. The Barbados Eye Studies Group.* Arch Ophthalmol, 2001. **119**(1): p. 89-95.
15. Leske, M.C., et al., *Nine-year incidence of open-angle glaucoma in the Barbados Eye Studies.* Ophthalmology, 2007. **114**(6): p. 1058-64.
16. European Glaucoma Prevention Study, G., et al., *Predictive factors for open-angle glaucoma among patients with ocular hypertension in the European Glaucoma Prevention Study.* Ophthalmology, 2007. **114**(1): p. 3-9.
17. Founti, P., et al., *Risk Factors for Visual Field Deterioration in the United Kingdom Glaucoma Treatment Study.* Ophthalmology, 2020. **127**(12): p. 1642-1651.
18. Heijl, A., et al., *Reduction of intraocular pressure and glaucoma progression: results from the Early Manifest Glaucoma Trial.* Arch Ophthalmol, 2002. **120**(10): p. 1268-79.
19. Leske, M.C., et al., *Comparison of glaucomatous progression between untreated patients with normal-tension glaucoma and patients with therapeutically reduced intraocular pressures. The effectiveness of intraocular pressure reduction in the treatment of normal-tension glaucoma.* Am J Ophthalmol, 1999. **127**(5): p. 625-6.

471 20. *The Advanced Glaucoma Intervention Study (AGIS): 7. The relationship between control of*
472 *intraocular pressure and visual field deterioration.The AGIS Investigators.* Am J Ophthalmol,
473 2000. **130**(4): p. 429-40.
474 21. Brubaker, R.F., *The effect of intraocular pressure on conventional outflow resistance in the*
475 *enucleated human eye.* Invest Ophthalmol, 1975. **14**(4): p. 286-92.
476 22. Karyotakis, N.G., et al., *Manometric measurement of the outflow facility in the living human eye*
477 *and its dependence on intraocular pressure.* Acta Ophthalmol, 2015. **93**(5): p. e343-8.
478 23. Becker, B. and J.S. Friedenwald, *Clinical aqueous outflow.* AMA Arch Ophthalmol, 1953. **50**(5): p.
479 557-71.
480 24. Weekers, R., M. Watillon, and M. De Rudder, *Experimental and clinical investigations into the*
481 *resistance to outflow of aqueous humour in normal subjects.* Br J Ophthalmol, 1956. **40**(4): p.
482 225-33.
483 25. Langham, M.E., *A New Procedure for the Analysis of Intraocular Dynamics in Human Subjects.*
484 Exp Eye Res, 1963. **2**: p. 314-24.
485 26. Langham, M.E. and J.E. Eisenlohr, *A manometric study of the rate of fall of the intraocular*
486 *pressure in the living and dead eyes of human subjects.* Invest Ophthalmol, 1963. **2**: p. 72-82.
487 27. Moses, R.A., *The effect of intraocular pressure on resistance to outflow.* Surv Ophthalmol, 1977.
488 **22**(2): p. 88-100.
489 28. Thorburn, W., *Recordings of applanating force at constant intraocular pressure. V. Intraocular*
490 *volume changes due to changes in the content of aqueous humour.* Acta Ophthalmol (Copenh),
491 1973. **51**(3): p. 390-410.
492 29. Acott, T.S. and M.J. Kelley, *Extracellular matrix in the trabecular meshwork.* Exp Eye Res, 2008.
493 **86**(4): p. 543-61.
494 30. Schuman, J.S., et al., *Excimer laser effects on outflow facility and outflow pathway morphology.*
495 Invest Ophthalmol Vis Sci, 1999. **40**(8): p. 1676-80.
496 31. Acott, T.S., et al., *Normal and glaucomatous outflow regulation.* Prog Retin Eye Res, 2021. **82**: p.
497 100897.
498 32. Alvarado, J., et al., *Age-related changes in trabecular meshwork cellularity.* Invest Ophthalmol
499 Vis Sci, 1981. **21**(5): p. 714-27.
500 33. Grierson, I. and R.C. Howes, *Age-related depletion of the cell population in the human trabecular*
501 *meshwork.* Eye (Lond), 1987. **1 (Pt 2)**: p. 204-10.
502 34. Lutjen-Drecoll, E., H. Wiendl, and P.L. Kaufman, *Acute and chronic structural effects of*
503 *pilocarpine on monkey outflow tissues.* Trans Am Ophthalmol Soc, 1998. **96**: p. 171-91;
504 discussion 192-5.
505 35. Lutjen-Drecoll, E. and P.L. Kaufman, *Biomechanics of echothiophate-induced anatomic changes*
506 *in monkey aqueous outflow system.* Graefes Arch Clin Exp Ophthalmol, 1986. **224**(6): p. 564-75.
507 36. Yu, B.P., *Aging and oxidative stress: modulation by dietary restriction.* Free Radic Biol Med, 1996.
508 **21**(5): p. 651-68.
509 37. Sherratt, M.J., *Age-Related Tissue Stiffening: Cause and Effect.* Adv Wound Care (New Rochelle),
510 2013. **2**(1): p. 11-17.
511 38. Li, G., et al., *In vivo measurement of trabecular meshwork stiffness in a corticosteroid-induced*
512 *ocular hypertensive mouse model.* Proc Natl Acad Sci U S A, 2019. **116**(5): p. 1714-1722.
513 39. Li, G., et al., *Anti-fibrotic activity of a rho-kinase inhibitor restores outflow function and*
514 *intraocular pressure homeostasis.* Elife, 2021. **10**.
515 40. Li, G., et al., *Visualization of conventional outflow tissue responses to netarsudil in living mouse*
516 *eyes.* Eur J Pharmacol, 2016. **787**: p. 20-31.

517 41. Li, G., et al., *Pilocarpine-induced dilation of Schlemm's canal and prevention of lumen collapse at*
518 *elevated intraocular pressures in living mice visualized by OCT.* Invest Ophthalmol Vis Sci, 2014.
519 **55**(6): p. 3737-46.
520 42. Overby, D.R., et al., *The structure of the trabecular meshwork, its connections to the ciliary*
521 *muscle, and the effect of pilocarpine on outflow facility in mice.* Invest Ophthalmol Vis Sci, 2014.
522 **55**(6): p. 3727-36.
523 43. Lindsey, J.D. and R.N. Weinreb, *Identification of the mouse uveoscleral outflow pathway using*
524 *fluorescent dextran.* Invest Ophthalmol Vis Sci, 2002. **43**(7): p. 2201-5.
525 44. Last, J.A., et al., *Elastic modulus determination of normal and glaucomatous human trabecular*
526 *meshwork.* Invest Ophthalmol Vis Sci, 2011. **52**(5): p. 2147-52.
527 45. Wang, K., et al., *The relationship between outflow resistance and trabecular meshwork stiffness*
528 *in mice.* Sci Rep, 2018. **8**(1): p. 5848.
529 46. Wang, K., et al., *Trabecular meshwork stiffness in glaucoma.* Exp Eye Res, 2017. **158**: p. 3-12.
530 47. Raghunathan, V.K., et al., *Glaucomatous cell derived matrices differentially modulate non-*
531 *glaucomatous trabecular meshwork cellular behavior.* Acta Biomater, 2018. **71**: p. 444-459.
532 48. Sherwood, J.M., et al., *Measurement of Outflow Facility Using iPerfusion.* PLoS One, 2016. **11**(3):
533 p. e0150694.
534 49. Madekurozwa, M., et al., *Measurement of postmortem outflow facility using iPerfusion.* Exp Eye
535 Res, 2022. **220**: p. 109103.
536 50. David, R., et al., *Epidemiology of intraocular pressure in a population screened for glaucoma.* Br J
537 Ophthalmol, 1987. **71**(10): p. 766-71.
538 51. Klein, B.E., R. Klein, and K.L. Linton, *Intraocular pressure in an American community. The Beaver*
539 *Dam Eye Study.* Invest Ophthalmol Vis Sci, 1992. **33**(7): p. 2224-8.
540 52. Reina-Torres, E., et al., *The vital role for nitric oxide in intraocular pressure homeostasis.* Prog
541 Retin Eye Res, 2021. **83**: p. 100922.
542 53. Stamer, W.D. and T.S. Acott, *Current understanding of conventional outflow dysfunction in*
543 *glaucoma.* Curr Opin Ophthalmol, 2012. **23**(2): p. 135-43.
544 54. Cracknell, K.P., et al., *Melanin in the trabecular meshwork is associated with age, POAG but not*
545 *Latanoprost treatment. A masked morphometric study.* Exp Eye Res, 2006. **82**(6): p. 986-93.
546 55. Miyazaki, M., K. Segawa, and Y. Urakawa, *Age-related changes in the trabecular meshwork of*
547 *the normal human eye.* Jpn J Ophthalmol, 1987. **31**(4): p. 558-69.
548 56. Matsumoto, Y. and D.H. Johnson, *Trabecular meshwork phagocytosis in glaucomatous eyes.*
549 Ophthalmologica, 1997. **211**(3): p. 147-52.
550 57. Epstein, D.L., et al., *Experimental obstruction to aqueous outflow by pigment particles in living*
551 *monkeys.* Invest Ophthalmol Vis Sci, 1986. **27**(3): p. 387-95.
552 58. Stamer, W.D. and A.F. Clark, *The many faces of the trabecular meshwork cell.* Exp Eye Res, 2017.
553 **158**: p. 112-123.
554 59. Liton, P.B., P. Gonzalez, and D.L. Epstein, *The role of proteolytic cellular systems in trabecular*
555 *meshwork homeostasis.* Exp Eye Res, 2009. **88**(4): p. 724-8.
556 60. Aboobakar, I.F., et al., *Rare protective variants and glaucoma-relevant cell stressors modulate*
557 *Angiopoietin-like 7 expression.* Hum Mol Genet, 2023. **32**(15): p. 2523-2531.
558 61. Lee, C., et al., *In vivo estimation of murine iris stiffness using finite element modeling.* Exp Eye
559 Res, 2021. **202**: p. 108374.
560 62. Yemanyi, F., et al., *Dexamethasone and Glucocorticoid-Induced Matrix Temporally Modulate Key*
561 *Integrins, Caveolins, Contractility, and Stiffness in Human Trabecular Meshwork Cells.* Invest
562 Ophthalmol Vis Sci, 2020. **61**(13): p. 16.
563 63. Vahabikashi, A., et al., *Increased stiffness and flow resistance of the inner wall of Schlemm's*
564 *canal in glaucomatous human eyes.* Proc Natl Acad Sci U S A, 2019.

64. Safa, B.N., et al., *A Histomorphometric and Computational Investigation of the Stabilizing Role of Pectinate Ligaments in the Aqueous Outflow Pathway.* BioRxiv, 2023. **submitted**.
65. Gabelt, B.T., et al., *Aqueous humor dynamics and trabecular meshwork and anterior ciliary muscle morphologic changes with age in rhesus monkeys.* Invest Ophthalmol Vis Sci, 2003. **44**(5): p. 2118-25.
66. Millar, J.C., et al., *Strain and Age Effects on Aqueous Humor Dynamics in the Mouse.* Invest Ophthalmol Vis Sci, 2015. **56**(10): p. 5764-76.
67. Yelenskiy, A., et al., *Total Outflow Facility in Live C57BL/6 Mice of Different Age.* Biomed Hub, 2017. **2**(3): p. 1-10.
68. Li, G., et al., *Disease progression in iridocorneal angle tissues of BMP2-induced ocular hypertensive mice with optical coherence tomography.* Mol Vis, 2014. **20**: p. 1695-709.
69. Li, G., et al., *Trabodenoson, an Adenosine Mimetic With A1 Receptor Selectivity Lowers Intraocular Pressure by Increasing Conventional Outflow Facility in Mice.* Invest Ophthalmol Vis Sci, 2018. **59**(1): p. 383-392.
70. Li, G., et al., *Integral role for lysyl oxidase-like-1 in conventional outflow tissue function and behavior.* FASEB J, 2020. **34**(8): p. 10762-10777.
71. Sherwood, J.M., et al., *Measurement of Ocular Compliance Using iPerfusion.* Front Bioeng Biotechnol, 2019. **7**: p. 276.
72. Orfanidis, S.J., *Introduction to Signal Processing.* . 1996: Englewood Cliffs, NJ: Prentice Hall.
73. Schneider, C.A., W.S. Rasband, and K.W. Eliceiri, *NIH Image to ImageJ: 25 years of image analysis.* Nat Methods, 2012. **9**(7): p. 671-5.
74. Boussommier-Calleja, A., et al., *Physical Factors Affecting Outflow Facility Measurements in Mice.* Invest Ophthalmol Vis Sci, 2015. **56**(13): p. 8331-9.
75. Hendargo, H.C., et al., *Automated non-rigid registration and mosaicing for robust imaging of distinct retinal capillary beds using speckle variance optical coherence tomography.* Biomed Opt Express, 2013. **4**(6): p. 803-21.
76. Huang, Q., et al., *A new adaptive interpolation algorithm for 3D ultrasound imaging with speckle reduction and edge preservation.* Comput Med Imaging Graph, 2009. **33**(2): p. 100-10.
77. Mariampillai, A., et al., *Speckle variance detection of microvasculature using swept-source optical coherence tomography.* Opt Lett, 2008. **33**(13): p. 1530-2.
78. Poole, K.M., et al., *Quantifying the vascular response to ischemia with speckle variance optical coherence tomography.* Biomed Opt Express, 2014. **5**(12): p. 4118-30.
79. Choy, K.C., et al., *Open-source deep learning-based automatic segmentation of mouse Schlemm's canal in optical coherence tomography images.* Exp Eye Res, 2022. **214**: p. 108844.
80. Maas, S.A., et al., *FEBio: finite elements for biomechanics.* J Biomech Eng, 2012. **134**(1): p. 011005.

Acknowledgements

We gratefully acknowledge support from The BrightFocus Foundation (postdoctoral fellowship G2021005F, BNS), NIH (K99EY035360 (BNS), T32EY007092 (NSFG), R01EY030871 (AJF), P30EY006360, P30EY005722, R01EY031748 (CBR), R01EY031710 (CRE and WDS), 5R01EY030124 (WDS) the Alfred P. Sloan Foundation G-2019-11435 (NSFG), the Georgia Research Alliance (CRE), and Department of Veterans Affairs Rehab R&D Service Career Development Awards (AJF; CDA-2; RX002342).

Figures and Figure legends

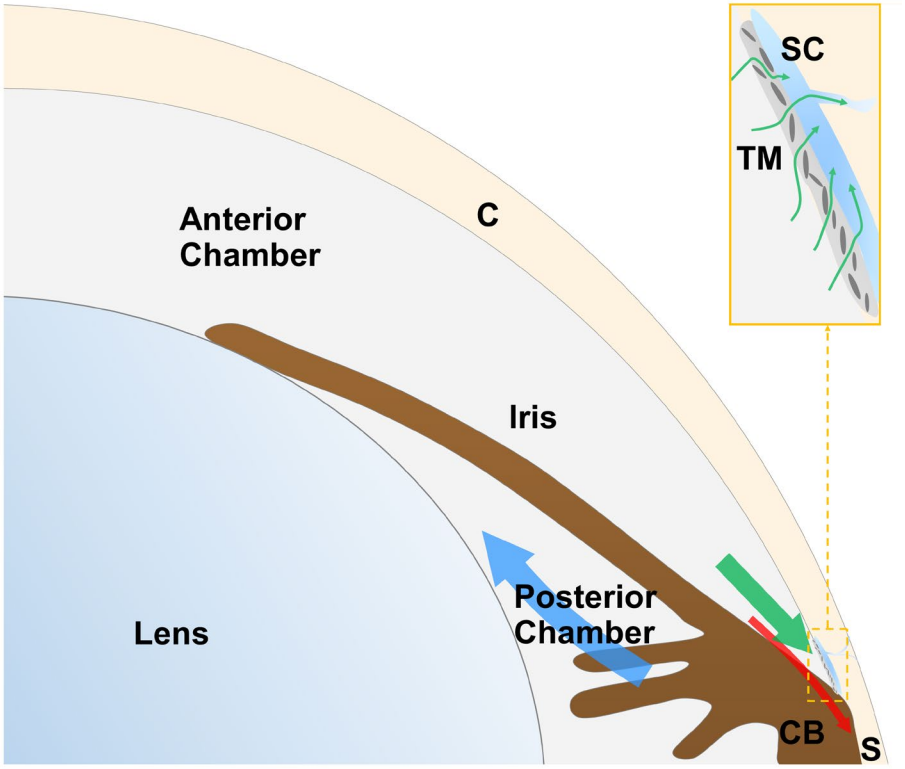

Figure 1: Schematic of the irideo-corneal angle of the mouse eye. The blue arrow is located in the posterior chamber, behind the iris, and shows the direction of aqueous humor flow after production by the ciliary body (CB). Aqueous humor enters the anterior chamber of the eye through the pupil, and then circulates in the anterior chamber before draining from the eye. The large green arrow shows the direction of aqueous humor flow out of the eye, primarily through the conventional outflow pathway (inset), and secondarily through the unconventional pathway (red arrow). The two key tissues of the conventional outflow pathway are the trabecular meshwork (TM), a porous connective tissue, and Schlemm's canal (SC), a specialized collecting vessel with an endothelial lining that has characteristics of both lymphatic and vascular endothelia. Additional abbreviations: Cornea (C) and Sclera (S).

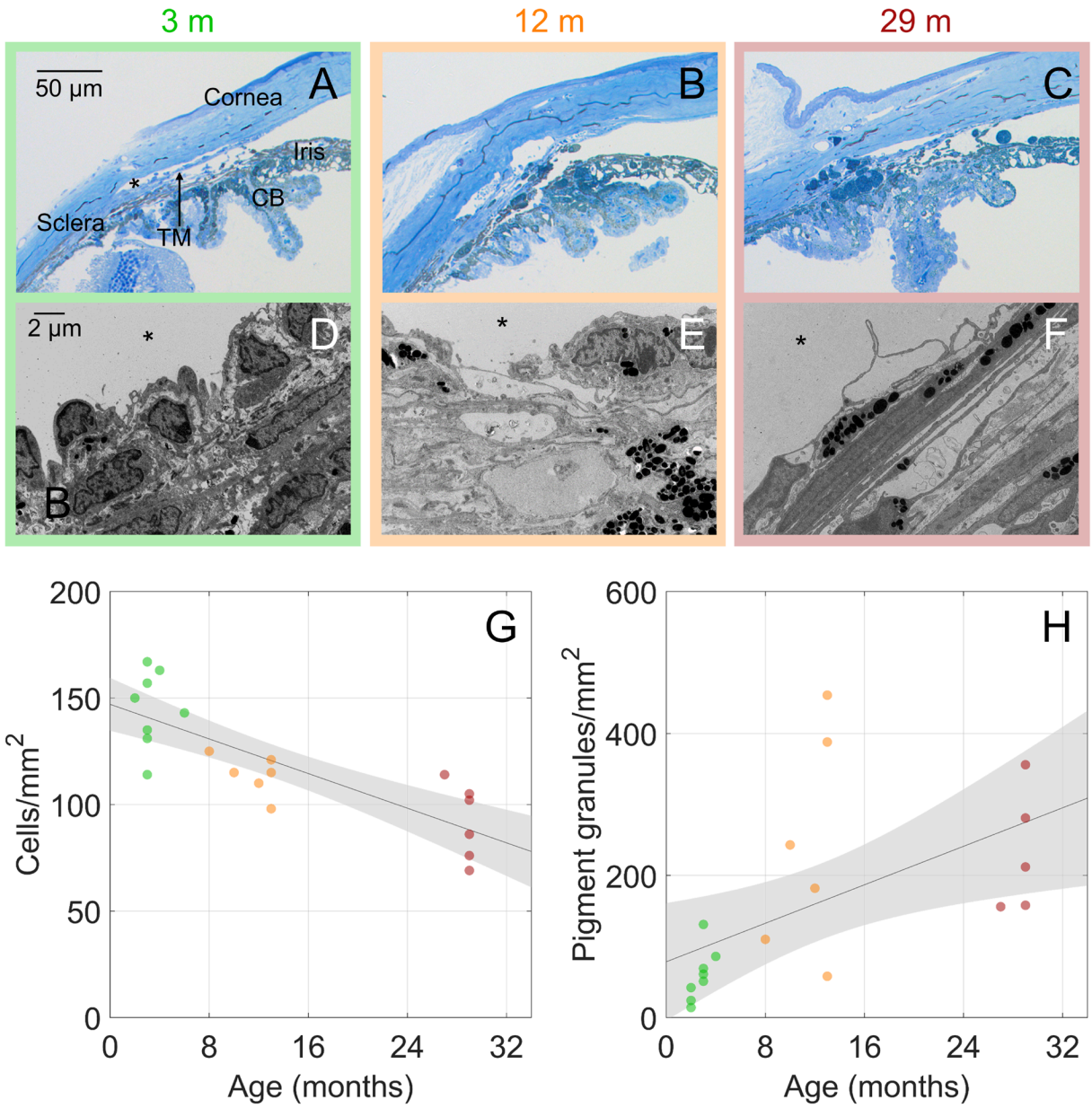

Figure 2. **Increased pigment and decreased cellularity were observed in the trabecular meshwork of older mouse eyes. A-F)** Representative histologic images (sagittal sections) of anterior segments from three different age groups of mice imaged by light microscopy (A-C) or transmission electron microscopy (D-F). While the gross structure of outflow tissues did not change with age, older eyes contained more pigment in the TM. * Denotes Schlemm's Canal lumen; images shown are representative and are from mice of 3, 12 and 29 months of age. **G)** The number of cell nuclei in the TM were counted in transmission electron micrographs (600×) and normalized by the visible TM area. An age-associated reduction in cellular density was evident ($R^2 = 0.66$, $p < 0.001$). **H)** The number of pigment granules within 7 µm of the inner wall of SC was counted and normalized to TM area. The density of pigment granules was weakly correlated with age ($R^2 = 0.32$, $p < 0.05$). Lines show best linear fits with grey shaded regions indicating the 95% confidence bands. Colors: green – young, orange – middle-aged, and red - elderly.

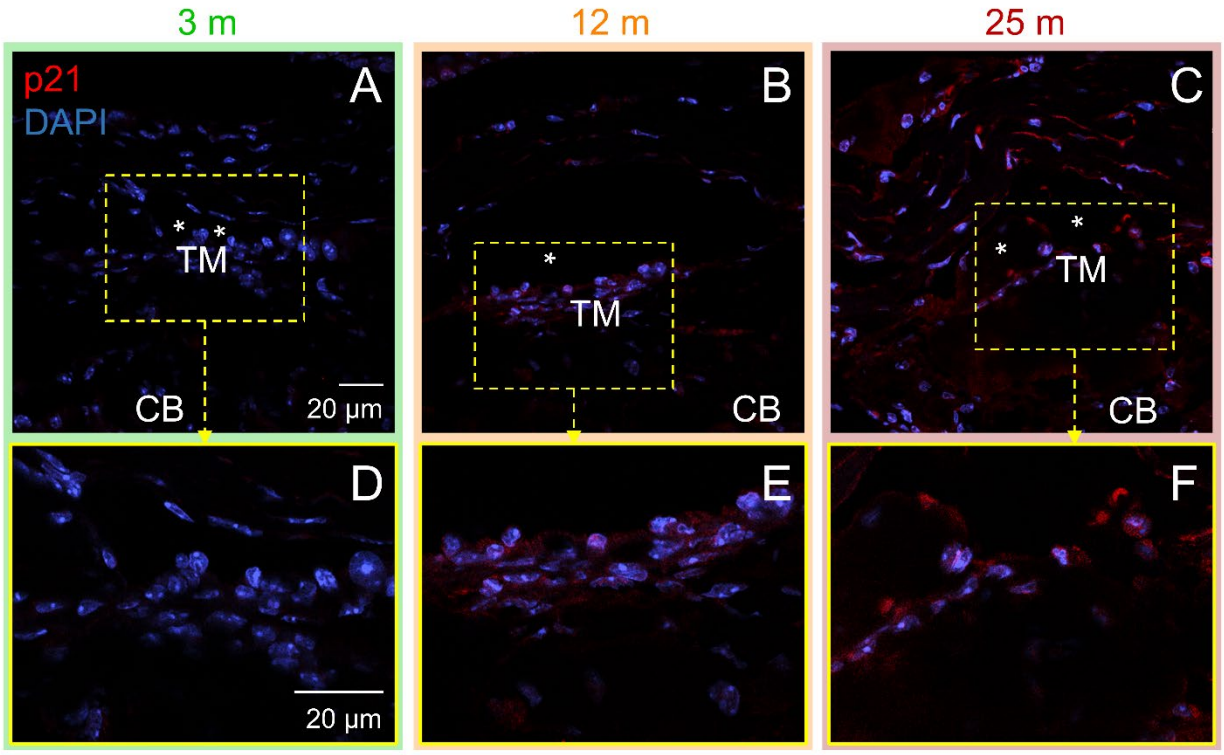

Figure 3. **Increased p21 expression is seen in outflow tissues of older mouse eyes.** Sagittal sections of outflow tissues from three age groups of mice (**A**: young, **B**: middle-aged and **C**: elderly) were immunostained with p21 antibody (red) and nuclei were labelled with DAPI (blue), then imaged by confocal microscopy, using the same settings for all images. The bottom row shows an enlargement of the region in the dashed box in the top row. * Denotes the lumen of SC; CB, ciliary body. Images are representative of N = 3 mice/age group.

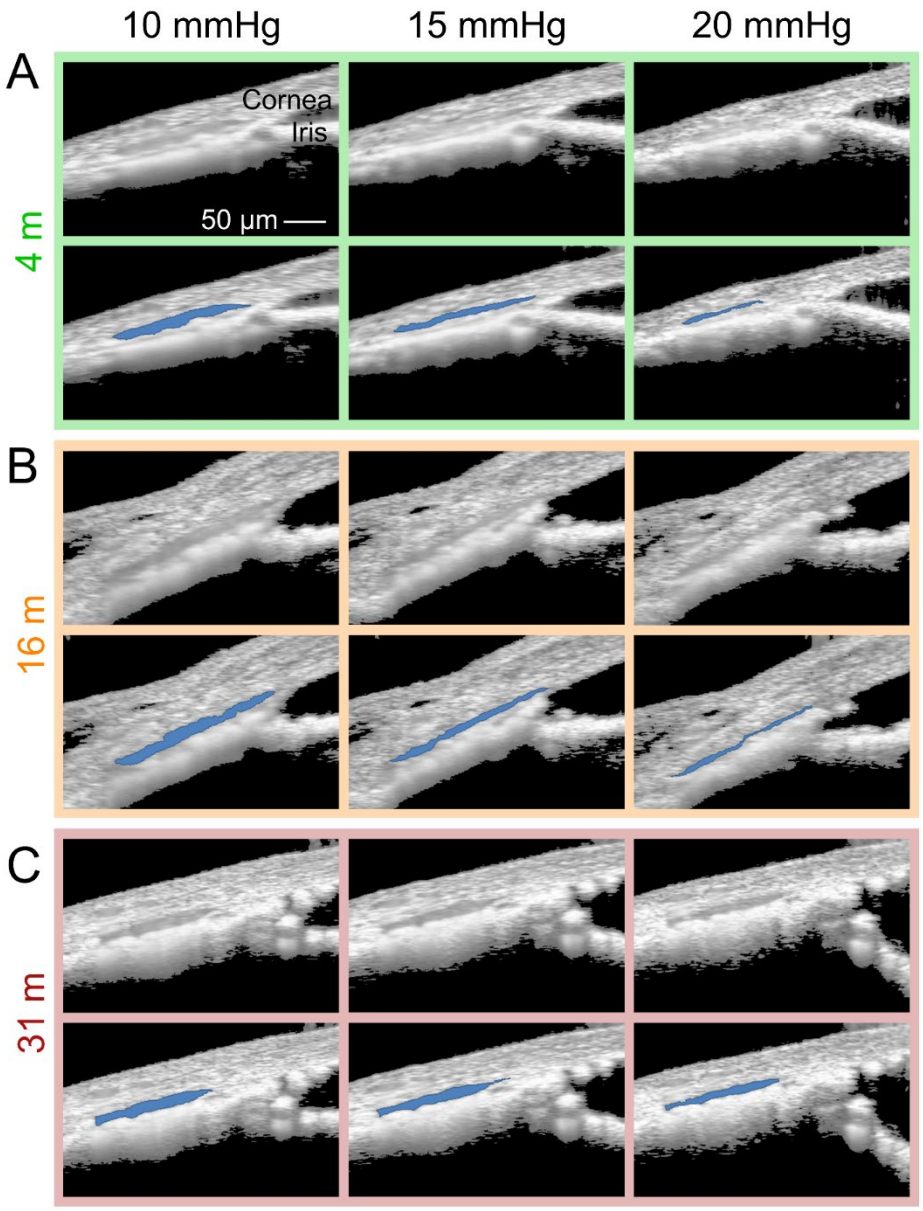

Figure 4. **Schlemm's canal is less susceptible to IOP-induced collapse in older mice.** The response of conventional outflow tissues to sequential intraocular pressure steps was visualized by spectral domain optical coherence tomography (SD-OCT) imaging. Representative images at three pressure steps (10, 15 and 20 mmHg) in three different age groups are shown. In each panel, the upper row shows the OCT image, and the lower row shows the same image in which SC lumen has been identified (blue) by our segmentation software. **A**: young, **B**: middle-aged and **C**: elderly.

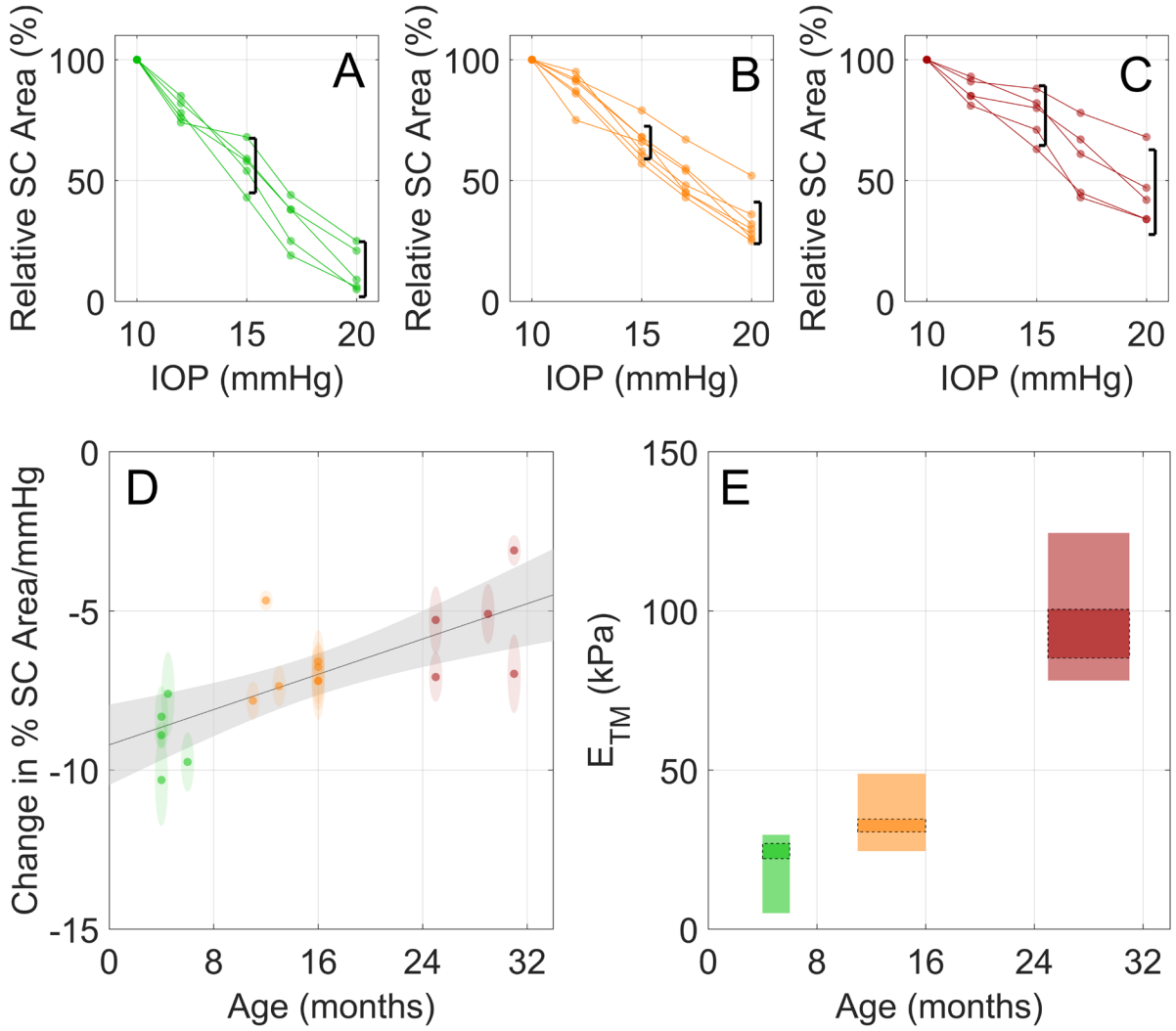

Figure 5. Quantification of reduced SC collapse and trabecular meshwork stiffening with age in mice. SC cross-sectional area was evaluated as a percentage of the baseline (10 mmHg) SC cross-sectional area for young (**A**), middle-aged (**B**) and elderly (**C**) mice, using images such as those shown in Figure 4. Lines connect data points for a given eye. Black brackets indicate 95% confidence intervals on Relative SC Area at 15 and 20 mmHg for all mice in the given age group, which were used as inputs for finite element modelling to determine effective TM stiffness. **D**) The slopes of the lines in panels A, B and C, computed using linear regression for each eye, are seen to be correlated with age ($R^2 = 0.55$, $p < 0.001$). Ellipse heights indicate 95% confidence intervals on the slopes and widths indicate age resolution of 1 month. Line shows the best linear fit with grey shaded region indicating the 95% confidence band. **E**) Trabecular meshwork stiffness was estimated by forward finite element modelling, as described in the text. The vertical limits of the rectangles indicate the range of TM stiffness (Young's modulus, E_{TM}) values that predict SC areas within the 95% confidence of the mean of the experimentally observed SC collapse, while widths indicate the age range of the experimental data. Rectangles with dashed outlines indicate Young's modulus values calculated when considering SC collapse as IOP was increased from 10 to 15 mmHg, while those without borders represent values calculated when considering SC collapse as IOP was increased from 10 to 20 mmHg. See Table S1 for plotted values. Colors: green – young, orange – middle-aged, and red - elderly.

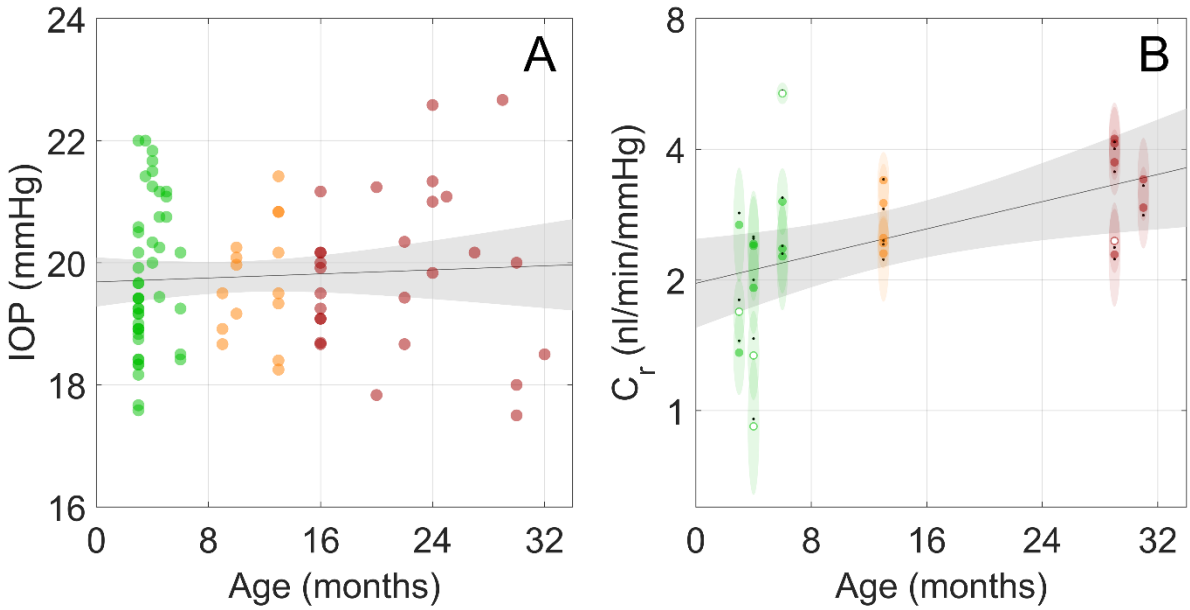

Figure 6. IOP and outflow facility were relatively insensitive to age. **A)** IOP was measured by tonometry. No correlation between age and IOP was observed ($R^2 = 0.00$, $p > 0.05$). **B)** Measured outflow facility showed a weak correlation with age ($R^2 = 0.26$, $p_B < 0.05$). Ellipse heights indicate 95% confidence intervals on facility and widths indicate the age resolution of 1 month. Hollow circles come from individual eyes while filled circles are averaged between both eyes from an animal. Black dots in panel B indicate adjusted facility values shown in Supplemental Figure 3A. Lines show best linear fits with grey shaded regions indicating the 95% confidence bands. Colors: green – young, orange – middle-aged, and red - elderly.

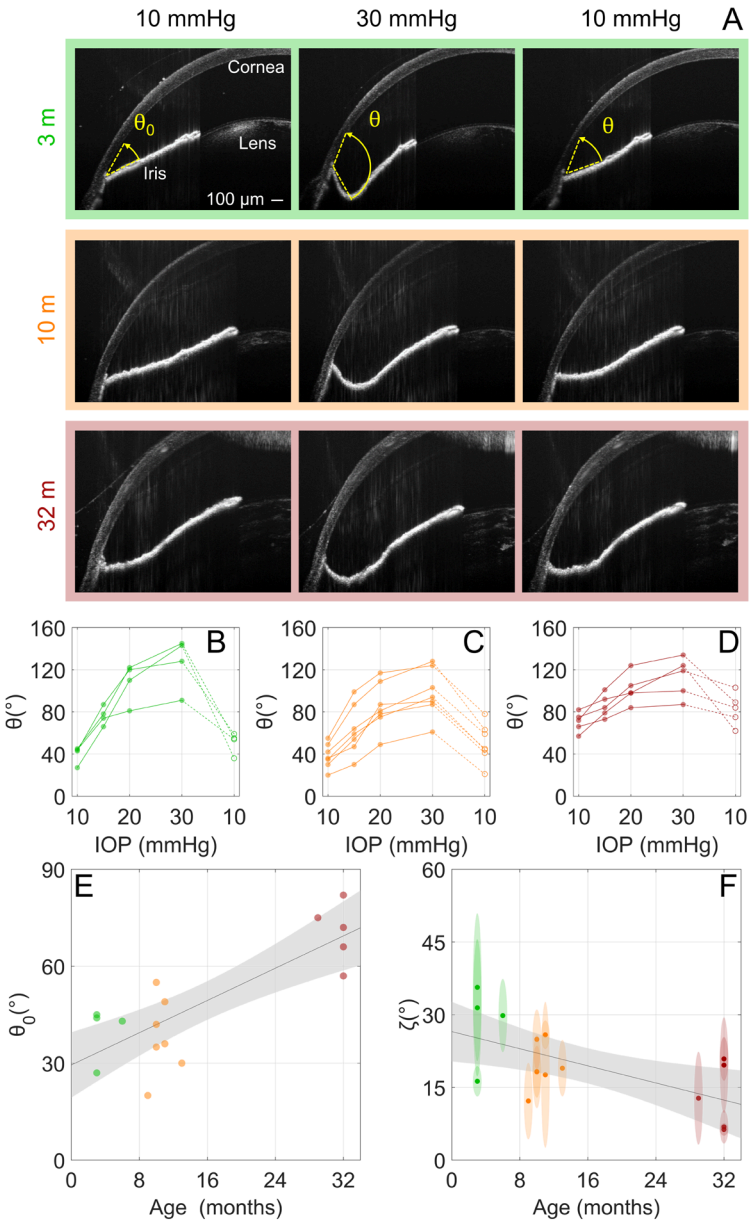

Figure 7. Iris deformations in response to increased IOP decreased with age in mice. A) Representative cross-sectional OCT images of mouse anterior segments in young, middle-aged and elderly mice. Images are shown (left to right) at the baseline IOP of 10 mmHg, at the peak IOP of 30 mmHg, and after returning to 10 mmHg. **B-D)** Quantitation of the irido-corneo angles at different IOPs from three age groups of mice (B: young, C: middle-aged and D: elderly). Connecting lines indicate individual eyes, and the dashed lines indicate the reduction in IOP back to the baseline of 10 mmHg. **E)** The irideo-corneal angle at the baseline IOP (10 mmHg, θ_0) was correlated with age ($R^2 = 0.64$, $p < 0.001$). **F)** The increase in irideo-corneal angle from baseline (θ-θ_0) was evaluated relative to the logarithm of the increase in IOP from baseline (P-P_0) with constant of proportionality ζ, which was calculated using regression. ζ represents the sensitivity of the irido-corneo angle to increasing IOP and was found to be negatively correlated with age ($R^2 = 0.38$, $p < 0.05$). Ellipse heights indicate 95% confidence intervals on ζ and widths indicate age resolution of 1 month. Lines show best linear fits with grey shaded regions indicating the 95% confidence bands. Colors: green – young, orange – middle-aged, and red – elderly.

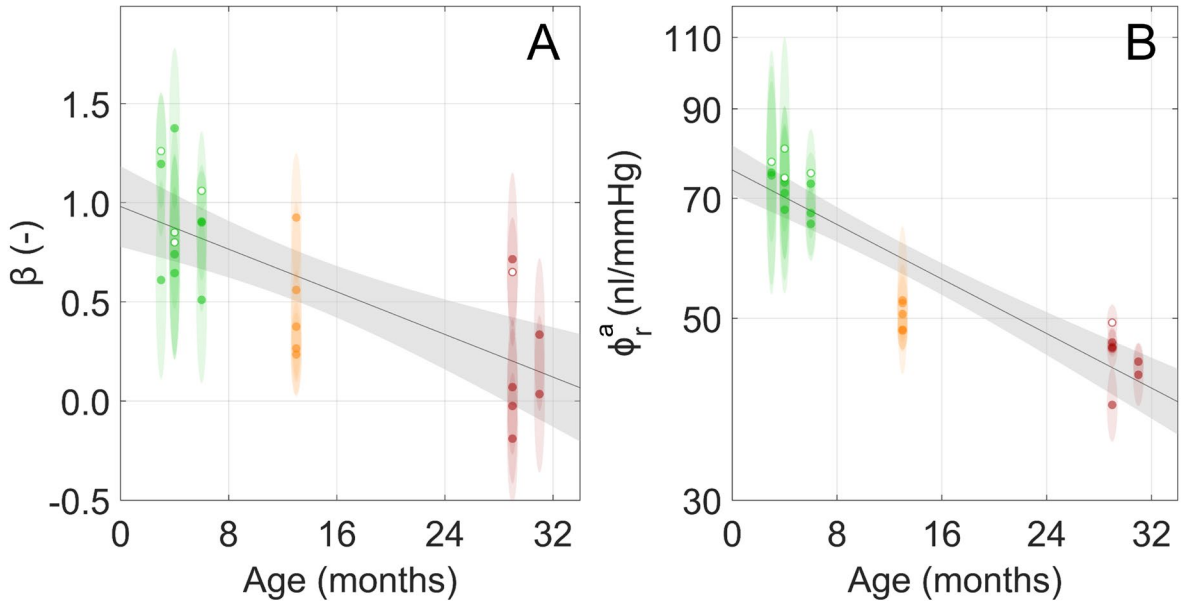

Figure 8. The pressure-dependence of outflow facility (β) and ocular compliance both decrease with age. A) A reduction in β, which represents the relative increase in outflow facility as pressure increases, was observed with increasing age ($R^2 = 0.51$, $p_B < 0.001$). Ellipse heights indicate 95% confidence intervals on β and widths indicate age resolution of 1 month. **B)** A strong negative correlation was observed between adjusted ocular compliance , $\phi_{r,i}^{a}$ (see text), measured via perfusion and adjusted for eye size to the expected compliance at 3.4 mm diameter, and age ($R^2 = 0.82$, $p_B < 0.001$).. Lines show best linear fits with grey shaded regions indicating the 95% confidence bands. Colors: green – young, orange – middle-aged, and red – elderly.